Journal Name

Dynamic Article Links ►

Cite this: DOI: 10.1039/c0xx00000x

www.rsc.org/xxxxxx

ARTICLE TYPE

Electronic Coupling in Iron Oxide-Modified TiO_2 Leads to a Reduced Band Gap and Charge Separation for Visible Light Active Photocatalysis

Michael Nolan*

Received (in XXX, XXX) Xth XXXXXXXXX 20XX, Accepted Xth XXXXXXXXX 20XX
DOI: 10.1039/b000000x

In recent experiments Tada *et al.* have shown that TiO_2 surfaces modified with iron oxide display visible light photocatalytic activity. This paper presents first principles simulations of iron oxide clusters adsorbed at the rutile TiO_2 (110) surface to elucidate the origin of the visible light photocatalytic activity of iron oxide modified TiO_2. Small iron oxide clusters adsorb at rutile (110) surface and their presence shifts the valence band so that the band gap of the composite is narrowed towards the visible, thus confirming the origin of the visible light activity of this composite material. The presence of iron oxide at the TiO_2 surface leads to charge separation, which is the origin of enhanced photocatalytic efficiency, consistent with experimental photoluminesence and photocurrent data. Surface modification of a metal oxide is thus an interesting route in the development of visible light photocatalytic materials.

Introduction

Harnessing renewable energy sources to provide future sources of energy for the planet is an area in which intense research efforts are underway. In particular utilising the vast amounts of solar energy freely available is considered key to removing humanity's dependence on finite fossil fuel sources. The development of new material systems to harness this energy is a crucial activity.

A cheap, readily available, stable and non-toxic material that can use visible light to produce hydrogen via photocatalytic water splitting is the goal of many research efforts. Prime candidate materials are titanium dioxide, TiO_2 and hematite, Fe_2O_3, which meet these criteria and have been well studied over recent years. However, both materials suffer from drawbacks that limit their applicability in visible light photocatalysis. For TiO_2, this drawback is that pristine TiO_2 has a band gap of 3 – 3.2 eV, depending on polymorph and sample treatment. Modifying TiO_2 to allow visible light photocatalysis has been the subject of many studies in recent years [1,2]. Hematite has a band gap in the visible, but has an extremely short charge diffusion length. For photocatalysis, both a suitable band gap for light absorption and good charge transport are required, while work in this field has tended to focus on band gap engineering, at least for TiO_2

Until recently, band gap engineering in TiO_2 has been dominant in this field and most efforts in modifying TiO_2 to enhance visible light absorption have focused on substitutional cation or anion doping at Ti or O sites [3-11], or cation-anion co-doping as a strategy to narrow the band gap [12-14]. While this has seen some level of success [14], there are still issues associated with simple substitutional doping of TiO_2, including dopant incorporation, stability and the nature of the electronic states formed. While most doping approaches do result in a material with a reduced band gap, dopants can lead to formation of localised electronic states that enhance electron/hole recombination, thus reducing the overall photocatalytic efficiency. While co-doping can in principle help with the last problem, see ref. 14, the overall issues associated with doping remain. Thus, there is a need to develop strategies for modification of TiO_2 that not only shift the band gap to the visible, but improve the photocatalytic efficiency, while alleviating issues associated with the doping process. While this question is a rather general one, we focus on TiO_2, since it is a leading candidate material, with a large body of existing work.

In achieving the goal of a material with visible light photocatalytic activity, there has arisen exciting research in an alternative approach, namely synthesising and characterising *composite* structures of a metal oxide supported on TiO_2. In particular, there have been interesting experiments describing composites of iron oxide and TiO_2 [15-18]. In these papers, the synthesis of iron oxide species (denoted FeO_x) supported on TiO_2 surfaces has been described. Most importantly, the resulting composites have been shown to demonstrate (i) visible light absorption and (ii) improved photocatalytic activity over pure TiO_2 and Fe_2O_3. Both band gap narrowing and improved charge, i.e. electrons and holes, separation have been claimed. The origin of this dramatic improvement over pure TiO_2 is postulated to arise from the relative positions of the TiO_2 and FeO_x electronic states, with Tada and co-workers suggesting that the iron oxide states form a new band above the top of the TiO_2 valence band (VB), leading to an upward shift of the composite VB and a band gap narrowing [17, 18]. With the conduction band (CB) states arising from TiO_2, this band alignment will result in separation of electrons and holes onto TiO_2 and FeO_x [16]. The problem with the

small charge diffusion distance in iron oxide is also removed, since the molecular size of the iron oxide species [17, 18] means that the diffusion distance is the same as the size of adsorbed iron oxide.

While there are recent very interesting examples of conceptually similar systems [19-24], the iron oxide modified TiO_2 composites are, at present, well characterised and show great promise in meeting the criteria for a suitable visible light photocatalytic material system.

In these works, Libera *et al.* [16] have used atomic layer deposition to grow FeO_x clusters on TiO_2 and the cluster size has been controlled during deposition. In the work of Tada *et al.* [17,18], a chemisorption-calcination cycle is used to convert an $Fe(acac)_3$ precursor that was initially chemisorbed at TiO_2 into adsorbed FeO_x, thus modifying the surface of TiO_2. The adsorbed iron oxide is described as dispersed, molecular sized FeO_x species [17, 18]

In light of these experimental studies, it is vital to understand the microscopic origin of the visible light activity of these new composites, which is best achieved using first principles simulations, with density functional theory (DFT). Such studies are now recognised as an extremely valuable tool in unravelling the properties of complex materials systems.

In this regard, we have previously used DFT calculations to study small TiO_2 clusters adsorbed at the rutile (110) surface [25]. In that study we found that with the TiO_2 clusters adsorbed at the TiO_2 surface, the band gap of the composite is narrowed and electrons and holes are separated onto the surface and the adsorbed cluster, confirming the potential of such a composite as a visible light photocatalytic material.

In light of the recent experimental results on FeO_x-TiO_2 composites [15-18] and recent work on other oxide-oxide composites [19-24], we study in this paper FeO_x species adsorbed at the rutile (110) surface, namely FeO, $(FeO)_2$ and Fe_2O_3, with the aim of elucidating the origin of the improved visible light activity of FeO_x-TiO_2 composites over pure TiO_2. Such small, molecular sized metal oxide clusters are good models of the dispersed, molecular scale adsorbed species described by Tada *et al.* [17,18]. We find that the top of the VB in the composite is derived from iron oxide states, namely Fe 3d and O 2p, while the CB is derived from Ti 3d states in TiO_2. The coupling of the electronic states on TiO_2 and FeO_x results in an upshift in the VB and a narrowing of the band gap, while the nature of the electronic states confirms separation of electrons and holes will occur after visible light excitation.

Methods

In the calculations, we employ DFT corrected for on-site Coulomb interactions (DFT+U) and adsorb FeO, $(FeO)_2$ and Fe_2O_3 species at the rutile (110) surface and relax the ions. A number of different adsorption sites for each FeO_x species have been examined and some short *ab initio* molecular dynamics simulations have also been run at 500 K. In the FeO_x species, FeO and $(FeO)_2$ have a formal Fe^{2+} oxidation state and Fe_2O_3 has a formal Fe^{3+} oxidation state.

To model the rutile (110) surface, we use a three dimensional periodic slab model and a plane wave basis set to describe the valence electronic wave functions within the VASP code, version VASP5.2 [26]. The cut-off for the kinetic energy is 396 eV. For the core-valence interaction we apply Blöchl's projector augmented wave (PAW) method [27], with Ti described by 4 valence electrons and oxygen by 6 valence electrons. We use the Perdew-Wang91 approximation to the exchange-correlation functional [28]. k-point sampling is performed using the Monkhorst-Pack scheme, with a (2 x 1 x 1) sampling grid; this set up has been used in a number of papers.

For describing Fe and Ti 3d states, we have used the PW91 exchange-correlation functional and have also applied the DFT+U approach. DFT+U [29,30], adds a Hubbard U correction to describe reduced metal cation states, such as Ti^{3+} and is also needed in studying iron oxides [31]. The need for an approach like DFT+U or hybrid DFT (which is too costly in a plane wave basis set for the present calculations with up to 300 atoms) to describe electronic states of partially filled d shells in transition metals is well known and has been the subject of a number of papers [32-36]. U = 4.5 eV on Ti 3d states is suitable to describe oxidised and reduced Ti and is consistent with values of U in the literature. For Fe 3d, we use U = 6.5 eV and J = 1 eV, again typical values used in the literature. For the bare TiO_2 (110) surface, this gives a valence-conduction band energy gap of 2 eV, which is obviously underestimated with respect to experiment.

The rutile (110) surface is made up of neutral O-Ti-O tri-layers along the slab with rows of two-fold coordinated bridging oxygens terminating the slab, and in the next layer there are two types of Ti: 6-fold coordinated Ti and exposed 5-fold coordinated Ti. A (2 x 4) surface cell expansion is employed, while the slab is 6 O-Ti-O layers thick (18 atomic layers) and the vacuum gap is 12 Å. All calculations are spin polarised.

The bare TiO_2 surface, the iron oxide clusters adsorbed at TiO_2 clusters and the free iron oxide clusters are calculated in the same periodic supercell, with the same plane wave cut off energy, the same k-point sampling grid, the same DFT approach and the same PAW potentials, ensuring consistency between calculations. To study cluster adsorption, the clusters are positioned in a number of configurations at the (110) surface and then a full relaxation is performed within a fixed supercell. The adsorption energy is computed from

$$E^{ads} = E((FeO_x)\text{-}TiO_2) - \{ E(FeO_x) + E(TiO_2) \} \quad (1)$$

Where $E((FeO_x)_n\text{-}TiO_2)$ is the total energy of the cluster supported on the surface, and $E(FeO_x)$ and $E(TiO_2)$ are the total energies of the free cluster and the bare surface; a negative adsorption energy signifies that cluster adsorption is stable.

Results and Discussion

Figure 1 shows the atomic structure of FeO, $(FeO)_2$ and Fe_2O_3 adsorbed at the rutile (110) surface. The adsorption energies, computed relative to free FeO_x and TiO_2 are also given in figure 1 and are denoted E^{ads}. These adsorption energies are computed as 0 K energy differences, but serve to give an indication of the relative stability of adsorbed iron oxide structures. The negative adsorption energies signify that the iron oxide species are stable when adsorbed at the TiO_2 surface and the magnitude of the adsorption energy means that these species should be thermally stable. Since at finite temperature the entropy of the adsorbate plays a key role in determining its stability at the surface, we

have computed the rotational and translational contributions to the gas phase entropy (S) of $(FeO)_2$ and Fe_2O_3 clusters[37]. At a given temperature, the adsorbate will desorb if $T\Delta S > -E^{ads}$. For gas phase $(FeO)_2$, $T\Delta S$ at 298 K is 0.93 eV, while for gas phase Fe_2O_3 $T\Delta S$ at 298 K is 1.03 eV. Comparing with figure 1, adsorption of iron oxide at the TiO_2 (110) surface is still thermodynamically favoured.

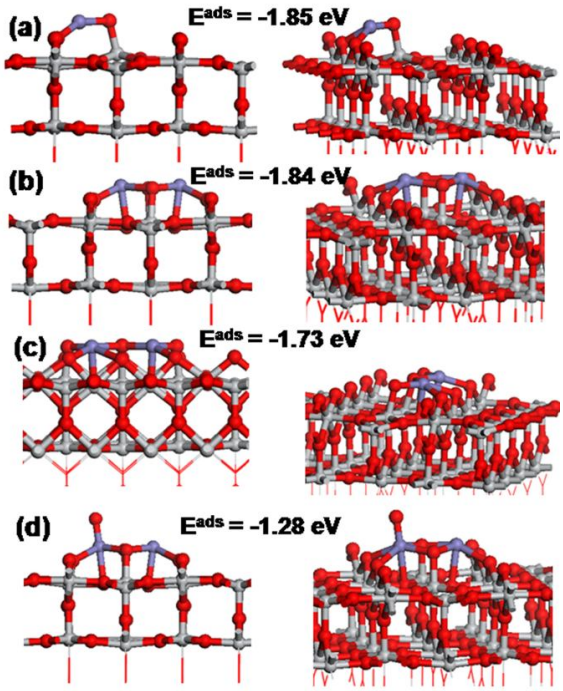

Fig. 1 Atomic structure of FeO_x adsorbed at the rutile TiO_2 (110) surface. (a) FeO, (b) $(FeO)_2$, (c) Fe_2O_3 Structure I and (d) Fe_2O_3 Structure II. In this, and in subsequent figures, Ti is the grey sphere, Fe is blue and O is red. The adsorption energies, in eV, are also given beside each structure.

For Fe_2O_3, we show two stable structures, highlighting that the strength of adsorption can be related to the number of new metal-O bonds formed between the cluster and the support. In Figure 1(c), the most stable adsorption structure of Fe_2O_3, has the O and Fe from iron oxide arranged in a zig-zag: O-Fe-O-Fe-O, typical of the most stable gas phase Fe_2O_3 cluster, and each O bonds to a 5fold coordinated Ti along one row in the TiO_2 surface; such a binding site for oxygen at the rutile (110) surface is known [38]. The Fe-O distances in adsorbed Fe_2O_3 are 1.82 Å and 1.93 Å; the latter oxygen is shared by Fe. The Fe-O distances to oxygen in TiO_2 are in the range 2.02 – 2.09 Å. Finally, the Ti-O distances involving oxygen from Fe_2O_3 are in the range 2.1 – 2.2 Å. In contrast to the most stable adsorption structure of Fe_2O_3, the structure in figure 1(d) has one oxygen from Fe_2O_3 bonded to a cluster Fe ion and with the loss of an O-Ti bond, the adsorption energy is more positive. For TiO_2 clusters, we found a similar relationship between the adsorption energy and the number of new metal-oxygen bonds formed upon adsorption [25].

FeO and $(FeO)_2$ have similar adsorption energies. In these adsorbed species, each Fe is bound to two bridging oxygen atoms of TiO_2, with Fe-O distances 2.01, 2.02 Å for adsorbed FeO and 2.11, 2.29 Å in adsorbed $(FeO)_2$. Oxygen from FeO and $(FeO)_2$ binds to a 5fold coordinated Ti atom from the surface, with Ti-O distances of 1.81 Å (FeO) and 1.89 Å ($(FeO)_2$). The Fe-O distances in the iron oxide cluster are 1.93 Å (FeO) and 2.04/2.12 Å ($(FeO)_2$).

Figure 2 shows the electronic density of states (PEDOS) projected onto Fe 3d and Ti 3d states for adsorbed FeO, $(FeO)_2$ and Fe_2O_3. The O 2p PEDOS plots (not shown) also display similar features for the relative positions of the FeO_x states and the TiO_2 states.

The PEDOS plots of FeO_x adsorbed at TiO_2 show that states from adsorbed FeO_x lie above the TiO_2 valence band, so that the iron oxide derived states lie at the top of the valence band. Therefore iron oxide adsorption at the TiO_2 surface has pushed the top of the valence band upwards in energy. The conduction band arises from the Ti 3d states. The consequences of the iron-oxide-TiO_2 electronic interactions are the following:

1 Since the valence band lies at higher energy, the band gap of the composite will be narrowed compared to pure TiO_2. Jin *et al.* [18] used XPS to claim that the top of the VB does indeed move to higher energies in the composite compared to pure TiO_2.

2 Although DFT+U underestimates the band gap of the composite, the shift in the valence band energy should be reasonably described. We determine an upward shift of the valence band edge so that the band gap narrowing is 0.3 eV, which will allow for visible light absorption in the composite. In ref. [17,18], the shift in the VB edge is determined to be 0.4 eV, which is consistent with the simulations

3 UV excitation from the TiO_2 valence band to the TiO_2 conduction band will still be present. In the experiments, an increase in UV activity is observed [18].

Upon visible light excitation, the alignment of the iron oxide and TiO_2 electronic states facilitates charge separation. In this scenario, after visible light excitation, electrons will be found on the TiO_2 support, while holes will be found on the iron oxide. This means that electrons and holes are naturally spatially separated, reducing the possibility of electron-hole recombination, increasing the photocatalytic activity and providing the origin of the experimental findings of enhanced photocatalytic activity in the composite. Even if UV light is used, so that the excitation is from the TiO_2 VB to CB (the VB-CB energy gap of TiO_2 is not significantly changed from the pure surface), the resulting holes will migrate to the iron oxide, which lies on the surface of TiO_2, and these holes will be available for further reaction.

Although it is not as widely discussed as band gap modulation, this aspect is extremely important for photocatalytic efficiency. Charge separation in FeO_x-TiO_2 was also discussed as an important benefit of forming the composite in the work of ref. [16], and photoluminescence and photocurrent spectra indicate that charge recombination in the composite will be reduced compared with pure TiO_2 [17,18,39].

To summarise our findings on the origin of improved visible light absorption of the iron-oxide TiO_2 composite, table 1 shows the offsets between the TiO_2 VB and CB edges and the FeOx states around the VB and CB. Thus, as an example, for $(FeO)_2$, the $(FeO)_2$ CB states lie 0.55 eV above the TiO_2 (110) CB edge, while the $(FeO)_2$ VB states lie 0.3 eV above the TiO_2 (110) VB edge. This leads to a reduced band gap over pristine TiO_2, due to

the highest occupied $(FeO)_2$ states lying higher in energy than the VB edge of TiO_2.

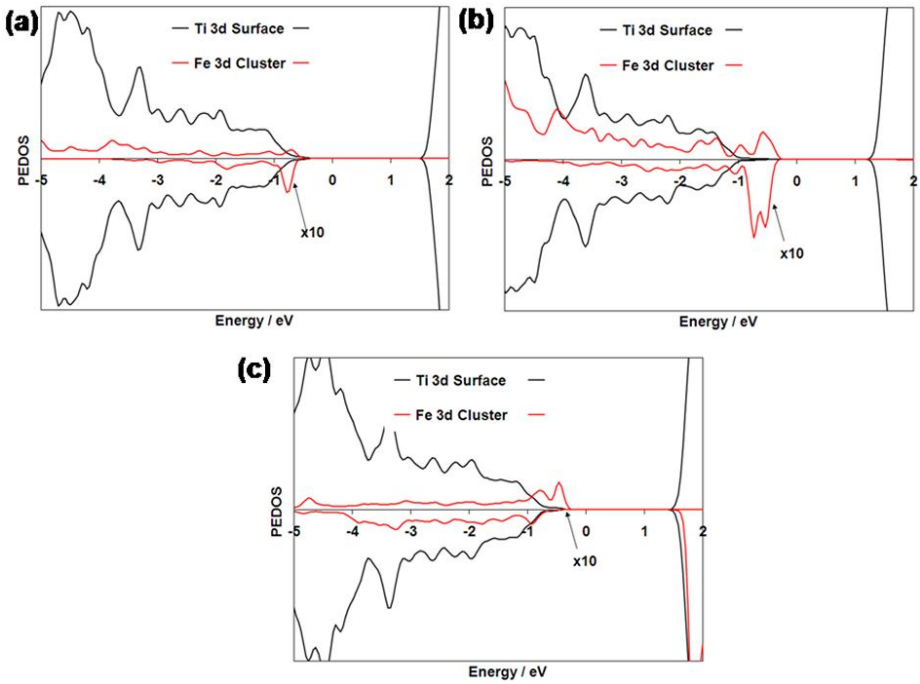

Fig. 2 Ti 3d and Fe 3d projected electronic density of states (PEDOS) for FeO_x adsorbed at the rutile TiO_2 (110) surface. (a) FeO, (b) $(FeO)_2$ Ti 3d and Fe 3d PEDOS, (c) Fe_2O_3 PEDOS for the most stable adsorption structure. The PEDOS for Fe in iron oxide are multiplied by 10 to facilitate comparison with the PEDOS from TiO_2.

On examining the electronic structure of free FeO clusters, the change from FeO to $(FeO)_2$ reduces the energy gap, shifting the lowest unoccupied electronic states of the cluster (the LUMO) to lower energy and the position of the highest occupied electronic state of the cluster (the HOMO) to higher energy; the HOMO shift is larger by 0.23 eV. The upwards shift in the occupied states going from FeO to $(FeO)_2$ is mirrored in the larger offset of the iron oxide VB to the TiO_2 VB for $(FeO)_2$ compared with FeO. It is also consistent with the smaller change on the relative position of the iron oxide LUMO states compared to the TiO_2 CB on going from FeO to $(FeO)_2$.

Table 1 Energy level offsets between the TiO2 VB/ CB and highest occupied FeOx states in FeO_x-TiO_2 composites, in eV. ΔE refers to the offset between the TiO_2 and FeO_x electronic states at the VB (ΔE^{VB}) or CB (ΔE^{CB}). A positive value signifies that the FeO_x state lies higher in energy than the TiO_2 derived state.

Structure	FeO-TiO_2	$(FeO)_2$-TiO_2	Fe_2O_3-TiO_2
$\Delta E^{(VB)}$	+0.15	+0.30	+0.3
$\Delta E^{(CB)}$	+0.60	+0.55	+0.1

To study further the nature of the iron and Ti species present in the composite, the excess spin density (which is the difference between the up spin and down spin electron density) is shown in figure 3. We have also computed Bader charges (since the PAW potentials are all-electron and it is possible to write the core charge from a PAW calculations) [40] and spin magnetisations; the latter provides information on the number of excess up spin over down spin electrons.

The Bader charges on Fe are as follows: FeO 6.54 electrons, and $(FeO)_2$ 6.52 electrons. This is consistent with an Fe^{2+} oxidation state ($3d^6$). The computed spin magnetisation on Fe is 4 spins, which is characteristic of an Fe^{2+} oxidation state, in which two of the six Fe $3d$ electrons are paired. In adsorbed Fe_2O_3 the Bader charges are 5.5 electrons, with computed spin magnetisations of 3 spins on each Fe; these are typical of an Fe^{3+} oxidation state. The excess spin density plots in figure 3 are consistent with Fe^{2+} and Fe^{3+}, showing an excess of electrons of one spin on each Fe in adsorbed FeO_x. There are no unpaired electrons on Ti in the surface; all Ti have computed Bader charges of 1.3 electrons, typical of a Ti^{4+} species and we have found no evidence of Ti^{3+} species.

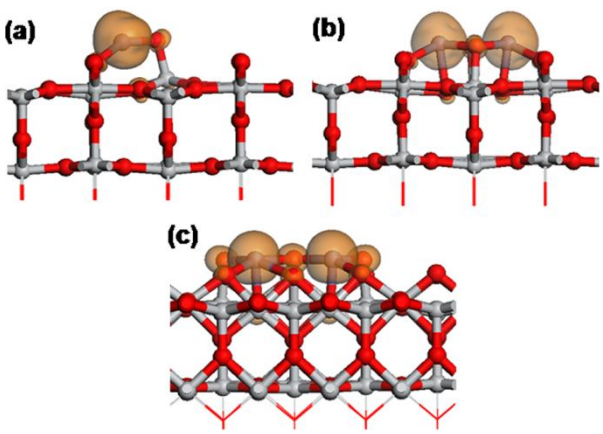

Fig. 3 Excess spin density for FeO_x adsorbed at the rutile TiO_2 (110) surface. (a) FeO, (b) $(FeO)_2$ and (c) Fe_2O_3.

In ref. [17,18] 2+ and 3+ oxidation states were found for Fe, which the authors of ref. [18] state arises from a mixed valence state for Fe. However, the present calculations indicate that irrespective of which oxidation state iron is found in, the modification of TiO_2 with iron oxide leads to a band gap reduction. The actual experimental conditions would determine which species are observed at a given time, e.g. during high energy X-ray irradiation to obtain XPS data, and one should expect the observation of Fe^{2+}/Fe^{3+} in the composite system to depend on experimental conditions.

Conclusions

In summary, we have presented first principles simulations of iron oxide clusters adsorbed at the rutile TiO_2 (110) surface to elucidate the origin of the visible light photocatalytic activity of iron oxide modified TiO_2. We find that small iron oxide clusters are stable at the TiO_2 surface and their presence leads to a narrowing of the band gap towards the visible, arising from the presence of iron oxide states lying above the valence band of the TiO_2. This confirms the origin of the visible light activity of this composite material. The presence of the iron oxide species at the TiO_2 surface also leads to charge separation, which is the origin of enhanced photocatalytic efficiency, consistent with experimental photoluminescence and photocurrent data. These initial experimental and modelling results indicate that surface modifications to metal oxides with oxide nanoclusters may be a fruitful route to developing visible light active photocatalyst materials.

Notes and references

[a] *Tyndall National Institute, University College Cork, Cork, Ireland; E-mail: michael.nolan@tyndall.ie*

† Electronic Supplementary Information (ESI) available: Coordinates of the most stable structures of iron oxide clusters adsorbed at the rutile (110) surface; in VASP CONTCAR format. See DOI:10.1039/b000000x/

This work is supported by Science Foundation Ireland (SFI) through the Starting Investigator Research Grant Program, project "EMOIN", grant number SFI 09/SIRG/I1620. We acknowledge computing resources at Tyndall provided by SFI and by the SFI and Higher Education Authority funded Irish Centre for High End Computing

1 A. Fujishima, X. Zhang and D. A. Tryk, *Surf. Sci. Rep.* 2008**, 63**, 515
2 X. L. Nie, S. P. Zhou, G. Maeng and K. Sohlberg, *Int. J. Photoenergy* 2009**,** 294042
3 Y. Cui, H. Du and L. S. Wen, *J. Mat. Sci. and Tech.*2008**, 24**, 675
4 H. W. Peng, J. B. Li, S. S. Li and J. B. Xia, *J. Phys. Cond. Matt.* 2008**, 20**, 125207
5 C. Di Valentin, G. Pacchioni, H. Onishi and A. Kudo, *Chem. Phys. Lett.* 2009**, 469**, 166
6 J. G. Yu, Q. J. Xiang and M. H. Zhou, *Appl. Cat. B Environmental* 2009**, 90**, 595
7 L. Bian, M. X. Song, T. L. Zhou, X. Y. Zhao and Q. Q. Dai, *J. Rare Earths* 2009**, 27**, 461
8 C. Di Valentin, E. Finazzi, G. Pacchioni, A. Selloni, S. Livraghi, M. C. Paganini and E. Giamello, *Chem. Phys.* 2007**, 339**, 44
9 A. M. Czoska, S. Livraghi, M. Chiesa, E. Giamello, S. Agnoli, G. Granozzi, E. Finazzi, C. Di Valentin and G. Pacchioni, *J. Phys. Chem C* 2008**, 112**, 8951
10 R. Long and N. J. English, *J. Phys. Chem. C* 2010**, 114**, 11984
11 J. W. Zheng, A. Bhattcahrayya,P. Wu, Z. Chen, J. Highfield, Z. L. Dong and R. Xu, *J. Phys. Chem. C* 2010**, 114**, 7063
12 Y. Q. Gai, J. B. Li, S. S. Li, J. B. Xia and S. H. Wei, *Phys. Rev. Lett.* 2009**, 102**, 036402
13 W. G. Zhu, X. F. Qiu, V. Iancu X. Q. Chen, H. Pan, W. Wang, N. M. Dimitrijevic, T. Rajh,H. M. Meyer, M. P. Paranthaman, G. M. Stocks, H. H. Weitering, B. H. Gu, G. Eres and Z. Y. Zhang, *Phys. Rev. Lett.* 2009**, 103**, 2264101
14 J. Zhang, C. X. Pan, P. F. Fang, J. H. Wie and R. Xiong, *ACS Applied Materials and Interfaces* 2010**, 2**, 1173
15 L. Peng, T. Xie, Y. Lu, H. Fan and D. Wang *Phys. Chem. Chem. Phys*. 2010, **12,** 8033
16 J. A. Libera, J. W. Elam, N. F. Sather, T. Rajh and N. M. Dimitrijevic, *Chem. Mat.*, 2010, **22**, 409
17 H. Tada, Q. Jin, H. Nishijima, H. Yamamoto, M. Fujishima, S-i. Okuoka, T. Hattori, Y. Sumida and H. Kobayashi, *Angew Chem. Int. Ed.* 2011, **50,** 3501
18 Q. Jin, N. Fujishima and H. Tada, *J. Phys. Chem. C* 2011, **115,** 6478
19 S. D. Tilley, M. Cornuz, K. Sivula and M. Graetzel, *Angew. Chem. Intl. Ed*., 2010, **49**, 6405
20 O. Bondarchuk, X. Huang, J. Kim, B. D. Kay, L. S. Wang, J. M. White and Z. Dohnalek, *Angew. Chem., Int. Ed*., 2006, **45**, 4786
21 J. A. Rodriguez and J. Hrbek, *Surf. Sci.*, 2009, **604**, 241
22 J. A. Rodriguez and D. Stacchiola, *Phys. Chem. Chem. Phys*., 2010, **12**, 9557
23 T. Onfroy, G. Clet and M. Houalla, *J. Phys. Chem. B*, 2005, **109**, 14588
24 N. Soultanidis, W. Zhou, A. C. Psarras, A. J. Gonzalez, E. F. Illiopoulou, C. J. Kiely, I. E. Wachs and M. S. Wong, *J. Am. Chem. Soc.*, 2010, **132**, 13462
25 A. Iwaszuk and M. Nolan, *Phys. Chem. Chem. Phys.* 2011**, 13***,* 4963
26 G. Kresse and J. Hafner, *Phys. Rev. B,* 1994, **49**, 14251; G. Kresse and J. Furthmüller, *Comp. Mat. Sci* 1996, **6**, 5
27 P. E. Blöchl, *Phys. Rev. B*, 1994, **50**, 17953; D. Joubert and G. Kresse, *Phys. Rev. B,* 1999, **59**, 1758
28 J. P. Perdew, J. A. Chevary, S. H. Vosko, K. A. Jackson, M. R. Pederson, D. J. Singh and C. Fiolhais, *Phys. Rev. B* 1993, **46***,* 6671
29 V. I. Anisimov, J. Zaanen and O. K. Andersen, *Phys. Rev B* 1991, **44**, 943
30 S. L. Dudarev, G. A. Botton, S. Y. Savrasov, C. J. Humphreys and A. P. Sutton, *Phys. Rev. B* 1998**, 57**, 1505
31 P. Liao and E. A. Carter, *J. Mat. Chem.,* 2010, **20,** 6703
32 B. J. Morgan and G. W. Watson, *J. Phys. Chem. C,* 2010**, 114***, 2321*
33 M. Nolan, S. Grigoleit, D. C. Sayle, S. C. Parker and G. W. Watson, *Surf. Sci.* 2005*,* **576**, 1200
34 S. Fabris, G. Vicario, G. Balducci, S. de Gironcoli and S. Baroni, *J. Phys. Chem. B* 2005*,* **109**, 22860
35 G. Pacchioni, *J. Chem. Phys.,* 2008*,* **128***,* 182505
36 P. R. de Moreira, F. Illas and R. L. Martin *Phys. Rev. B* 2002, **65**, 155102
37 PW. Atkins, Physical Chemistry, 4th ed.; Oxford University Press: New York, 2004.
38 A. Greuling, P. Rahe, M. Kaczmarski, A. Kühnle and M. Rohlfing, *J. Phys. Condens. Matt.,* 2010**,** 22*,* 345008
39 A study of Bi_2WO_6-TiO_2 has highlighted charge separation through photolumisence spectra. Q. C. Xu, D. V. Wellia, Y. H. Ng, R. Amal and T. T. Y. Tan *J. Phys. Chem. C* 2011, **115,** 7419
40 G. Henkelman, A. Arnaldsson and H. Jónsson, Comput. Mater. Sci., 2006, 36, 254. In the VASP calculations, the PAW potentials used, as detailed in section 2, are all-electron potentials, with a frozen core. Thus, it is possible to do a Bader analysis, through using the LAECHG flag in VASP, which includes core charge density in the VASP CHGCAR file and we have then used the Bader code from Henkleman's group to perform the Bader analysis. A description is given at the following URL: http://theory.cm.utexas.edu/vtsttools/bader/vasp.php.